Chinese Chemical Letters 36 (2025) 110009

Contents lists available at ScienceDirect

Chinese Chemical Letters

journal homepage: www.elsevier.com/locate/cclet

Solid-acid-Lewis-base interaction accelerates lithium ion transport for uniform lithium deposition

Ruofan Qi, Jing Zhang, Wang Sun, Yu Bai, Zhenhua Wang*, Kening Sun

Beijing Key Laboratory of Chemical Power Source and Green Catalysis, School of Chemistry and Chemical Engineering, Beijing Institute of Technology, Beijing 100081, China

ARTICLE INFO

Article history:
Received 13 March 2024
Revised 25 April 2024
Accepted 13 May 2024
Available online 15 May 2024

Keywords:
Acid-base interaction
Mesoporous molecular sieve
Separator
Li-ion transference number
Lithium metal battery

ABSTRACT

Lithium metal batteries, with their light mass anode and high theoretical specific capacity of 3860 mAh/g, have great potential for development in achieving high energy density. However, the generation of lithium dendrites and the loss of dead lithium pose a serious threat to the safety and long-cycle stability of batteries. Herein, we utilize the Lewis acid-base interaction principle for lithium-ion migration regulation. Through loading solid-acids onto molecular sieves to immobilize Lewis base (PF_6^-), we achieve accelerated dissociation of lithium salts and successfully increase the lithium ion transference number to 0.44. Lewis acid-base interaction helps lithium metal batteries achieve more uniform lithium deposition, with an average CE improved to 92.8%. The symmetrical cells can be plated/stripped stably for more than 800 h of cycling. Full cell with high surface-loaded LFP cathode (14 mg/cm^2) exhibits impressively high capacity retention of 90.7% after 120 cycles at 0.5 C.

The current batteries with intercalated electrode materials as electrodes have limited performance improvement in terms of mass and bulk density. Lithium metal battery (LMB) has received much attention due to its theoretical specific capacity of 3860 mAh/g [1-3] and its low redox potential of 3.04 V (*vs.* standard hydrogen electrodes) [4,5]. Nevertheless, significant challenges remain in the development and application of lithium metal batteries.

One of the fundamental problems is the non-uniformity of lithium ion flux [6,7], where deposited lithium (Li) turns to form dendrites on the anode, which can puncture the separator and cause thermal runaway and other safety hazards [8-11]. The fracture and peeling of dendrites can lead to the accumulation of dead lithium, resulting in an irreversible capacity loss leading to a shorter cycle life of the battery [12-14]. Therefore, it is important that lithium-ions are transported uniformly and conveniently in the bulk phase and near the lithium metal surface. In recent years, many approaches involving separator modification [15-18], lithium metal anode modification [19-21], electrolyte regulation [22-24] and the use of solid electrolytes with high ionic conductivity [25-28] have been taken to improve lithium-ion transport.

Among them, the separator surface coating modification technology is simple and easy to implement, various materials have been explored for coating the separator, such as organic polymers [29,30], inorganic oxides [31,32], ceramic materials [33,34], composite materials [35], organic frame materials [36,37]. For example, the lithium-based metal-organic-framework (Li-MOF) [38] or TaO_3 nanosheets [39], *etc.* were coated onto the polypropylene separator, utilizing the spatial limitations of the pore structure to allow only Li^+ to pass through, while blocking the larger anion and improving anode deposition. Ceramic materials such as the solid-state fast ionic conductor LLZTO [40] also have three-dimensional ion channels, which can act as redistributors to regulate lithium ion transport and homogenize lithium ion flow. Zhao *et al.* [41] designed a coating of spherical mesoporous molecular sieve nanoparticles to modulate the solvation structure of lithium ions and reduce the desolvation energy. Therefore, separator coating modification can result in uniform transport of lithium ions, with improved wettability and mechanical strength.

During ions transport, anions in the electrolyte salts usually do not participate in the lithiation reaction but account for a high percentage of the mobility, leading to greater concentration polarization [42,43]. Recently, researchers have found that immobilizing some of the liquid electrolyte's anions will help stabilize electrodeposition and extend battery life [44-46]. For instance, separators with polar carboxyl groups immobilize anions by hydrogen bonding and accelerate Li^+ transport by desolvation [47]. Hao *et al.* [48] utilized the inherent -NH_2 group in MOFs to interact with anions; meanwhile, the channels between MOFs were modified by negatively charged -SO_3^-, which was electrostatically repulsive to an-

* Corresponding author.
E-mail address: wangzh@bit.edu.cn (Z. Wang).

https://doi.org/10.1016/j.cclet.2024.110009
1001-8417/

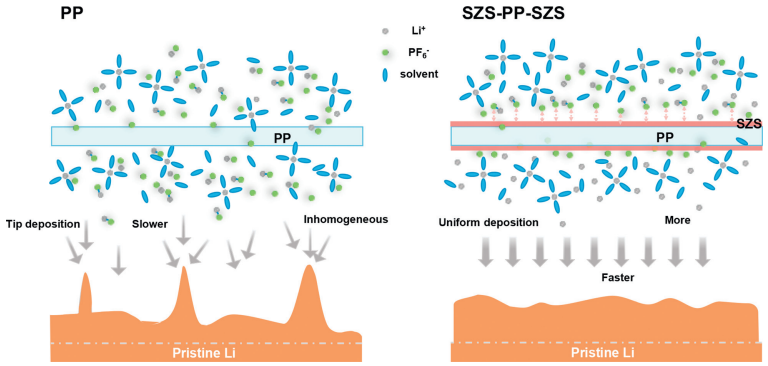

Fig. 1. Schematic comparison of anode deposition for batteries with PP separators (left) and SZS-PP-SZS modified separators (right).

ions, thus restricting the free migration of anions and facilitating lithium ion transport. What is more, a variety of solid-state electrolytes [49-51] and electrolyte engineering [52-55] have also been developed to anchor anions, promote lithium salt dissociation, and enhance Li^+ transference number by designing different acidic active sites.

In this work, we loaded solid acid upon mesoporous molecular sieves (SBA-15) and applied them to lithium metal battery systems. Mesoporous molecular sieves have very large specific surface area and pores, they are used to provide sufficient active sites and uniform the lithium ion flow [56,57]. The solid acid of sulfated zirconia (ZrO_2/SO_4^{2-}, recorded as SZ) has greater acidity and the stronger electron-absorbing ability, which improves the affinity of the materials for Lewis bases, promotes the dissociation of lithium salt lithium hexafluorophosphate ($LiPF_6$), anchors PF_6^- anion, and serves to increase the Li^+ transference number (Fig. 1). The modified separator (SZS-PP-SZS) coated with solid-acid loaded mesoporous molecular sieve composites (SZS) enables the t_{Li^+} to reach 0.44. SEM images display that the growth of lithium dendrites is largely inhibited. Increased ion transport leads to more uniform Li deposition, ensuring higher Coulombic efficiency (CE) and stable cycling of over 800 h for lithium metal symmetrical cells.

ZrO_2/SO_4^{2-} solid-acids (SZ) were loaded on SBA-15 mesoporous molecular sieves using the equal volume impregnation-calcination method (Fig. S1 in Supporting information). The acid loading does not change the overall morphology of the mesoporous molecular sieves (Fig. S2b in Supporting information). Nitrogen adsorption and desorption curves show that different acid loadings could significantly affect the porosity and pore size of mesoporous molecular sieve channels (Fig. S3 in Supporting information). The pore volume of SBA-15 mesoporous molecular sieve is approximately 1.31 cm^{-3} g^{-1}, and the pore diameter is approximately 7.91 nm. The pore volume and diameter of 20% loading composite material is 0.72 cm^{-3} g^{-1} and 7.83 nm, respectively. The surfaces of the composite separators are denser compared with that of the polypropylene separators (Figs. S4a and b in Supporting information), which effectively improve the disadvantage of uneven Li^+ distribution by the large and uneven pores of the PP separators. The ionic conductivity of 20% loading SZS-PP-SZS reached 1.40 mS/cm, which was much higher than the 0.69 mS/cm of the PP separator (Fig. 2a and Fig. S5 in Supporting information). By the way, pure SBA molecular sieves instead has a higher conductivity due to a larger pore size and not immobilizing anions. In addition, the inorganic material coating significantly scaled up the poor wettability of the PP separators in the carbonate electrolyte (Fig. S4c in Supporting information). The contact angle of the SZS-PP-SZS separator is 17.2°. The contact angle of the 20% loading SZS-PP-SZS is only 14.9° compared to 68.9° for the PP separator. The improved wettability reduced the interfacial impedance of the cells and enhanced the ion diffusion capability.

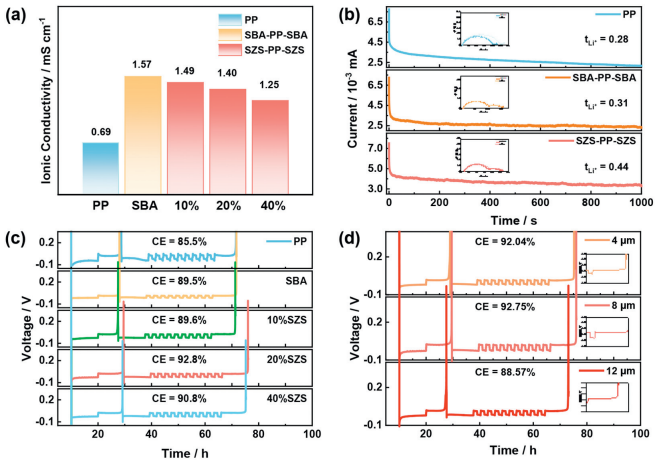

Fig. 2. (a) The ionic conductivity of PP, SBA and SZS-PP-SZS of different acid loadings. (b) Li^+ transference numbers and the chronoamperometry profiles of Li||Li symmetrical coin cells with PP, SBA, SZS-PP-SZS (optimum 20%) separators. (c) Average CE of Li||Cu half-cells with PP, SBA and different acid loadings SZS-PP-SZS. (d) Average CE of SZS-PP-SZS (optimum 20%) separators with different thicknesses.

The t_{Li+} of the SZS-PP-SZS separators reached 0.44, while that of the PP separators was only 0.28 (Fig. 2b). More and more uniform lithium-ions transport enabled more efficient replenishment of lithium-ions at the electrode interface, resulting in more uniform lithium deposition as well. The average CE of the Li||Cu battery with the 20% loading SZS-PP-SZS composite separator is as high as 92.8%, compared to 85.5% for PP (Fig. 2c) [58]. The SZS-PP-SZS cells exhibited lower polarization potential than that of the PP in both the initial lithium plating/peeling process and the later cycles. Moreover, the average CE test result of the cells assembled with separators coated only with SBA molecular sieves is 89.5%, which is not a significant improvement. For all comparisons, 20% acid loading is the optimum ratio. SBA-15 molecular sieves and composites further loaded with solid-acid are consistent in the improvement of mobility number and coulombic efficiency.

The thicker the coating, the more liquid could be stored in the separator (Fig. S6 in Supporting information), but at the same time the ionic transport distance will be farther, which is equivalent to increasing the conductivity requirement. Eventually, combining the CE test about the different thickness separators (Fig. 2d) and liquid absorption rates, the separators with the thickness of 8 μm has the best modification effect than 4 μm and 12 μm (Figs. S4d-f in Supporting information). The liquid absorption rate of the SZS-PP-SZS separators under the optimal selection is 1.28 times that of the PP separators. The PP and SZS-PP-SZS separators were immersed in the electrolyte (1 mol/L $LiPF_6$ in EC/DMC, 3:7, v/v) for 12 h. We tested the electrolyte by PH test paper, and the results show that

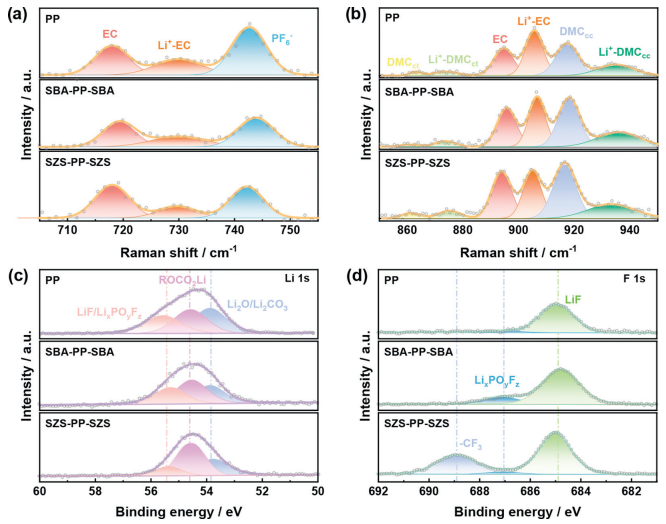

Fig. 3. (a, b) Raman spectra of electrolyte components of immersed PP separator (upper zone), SBA-PP-SBA (mid zone) separator and SZS-PP-SZS (lower zone) separator. XPS spectra of lithium metal electrodes after 5 cycles: (c) Li 1s and (d) F 1s.

the PH of the electrolyte corresponding to the PP and the SZS-PP-SZS was around 7 and 4, respectively (Fig. S14 in Supporting information).

The reason for the high Li^+ transference number of the SZS-PP-SZS composite separators was determined through Raman characterization. Under the influences of the mesoporous channel structure, lithium-ions are more evenly dispersed in the direction of transport through the separators. Together with the acid-base effect, the dissociation ability of $LiPF_6$ salt was enhanced, and the mutual binding between electrolyte solvents also changed. We immersed three separators in the electrolyte (1 mol/L $LiPF_6$ in EC/DMC, 3:7, v/v) for 12 h and then tested the electrolyte Raman spectrum (Figs. 3a and b). The electrolyte environment around the SZS-PP-SZS separator was different from that of the PP separator and SBA-PP-SBA separator. The results show that the peak intensities of PP and SBA-PP-SBA separators at 729.1 cm^{-1} are similar, but the intensity of SZS-PP-SZS separator is slightly lower (22.15% *vs.* 23.91% *vs.* 17.17%). The differences indicate that the molecular sieve structure don't change the solvated structure but the addition of solid-acids effect the binding of Li^+ and EC. At the same time, the ratios of the free PF_6^- anions (742.5 cm^{-1}) to free EC solvent molecules (717.6 cm^{-1}) are getting smaller and smaller under the three separators environments (intensity ratio PP-1.69 *vs.* SBA-1.28 *vs.* SZS-0.92) (Table S1 in Supporting information). Fig. 3b shows that the percentage of EC and DMC molecules increases after the anions are immobilized. This result is attributed to the premise that sufficient and rapid salt dissociation makes lithium ions to be released to participate in interfacial deposition replenishment, while anions are immobilized and the percentage of solvent molecules in the bulk phase not involved reaction is increased. Acid-base sites interactions between the separator and the electrolyte accelerate the dissociation of the $LiPF_6$ and anchor the anions. The composites loaded with solid-acids have a stronger acidic effect than molecular sieves, thus the Li^+ migration for cells with composite separators is increased significantly.

Acid-base interactions promote uniform and rapid transport of lithium-ions, resulting in a more homogeneous deposition process on the electrode surface. We activated the Li||Li symmetric cells with 3 cycles using a current of 0.5 mA/cm^2, then performed XPS testing of the SEI composition on the anode surfaces. In the Li 1s spectrum of Fig. 3c, the peaks located near 55.8 eV correspond to LiF and $Li_xPO_yF_z$, while the peaks near 54.6 eV correspond to organolithium. According to the peak area ratios in Table S3 (Supporting information, 0.84:0.67:0.31), the decrease of the LiF/$Li_xPO_yF_z$ percentage is attributed to the anchoring of anions by acid-base interaction. Besides, in the F 1s spectra of Fig. 3d, the small amount of intermediates $Li_xPO_yF_z$ (687.1 eV) appear in the anode surfaces of SBA-PP-SBA and SZS-PP-SZS. This result shows that trace amounts of water in the carbonate electrolyte react with PF_6^- bound to the SZ active sites [43], which further illustrates that SZ solid acids can effectively anchor PF_6^- at their active sites. Under the catalysis of SZ, PF_6^- decomposes to generate $PO_yF_z^-$, and a very small amount of $PO_yF_z^-$ leaves the anchor of SZ and migrates to the anode surface.

In order to investigate the effect of electrochemical kinetics of SZS-PP-SZS composite separators, activation energy tests were carried out on cells assembled with PP and SZS-PP-SZS separators, respectively. By testing the R_{ct} at different temperatures and fitting calculations (Figs. S9a and b in Supporting information), the interfacial charge transfer activation energy of the PP separator is 38.42 kJ/mol, whereas that of the SZS-PP-SZS separator is 27.92 kJ/mol. The reduction of activation energy in the charge transfer process proves that the SZS-PP-SZS separator accelerates the Li^+ electrochemical deposition on the anode surface. The lithium deposition on anode consumes lithium ions and causes concentration polarization. In batteries equipped with modified separators, the acceleration of charge transfer and the release of more Li^+ transport from the bulk phase weaken the concentration polarization. This reduces the tip effect and inhibites dendritic lithium deposition. Another aspect, due to the increase of the number of Li^+ migration, the activation energy of the Li^+ across the SEI membrane decreases from 59.79 kJ/mol in PP cell to 50.18 kJ/mol in SZS-PP-SZS cell (Figs. S9a and c in Supporting information). Likewise, the enhancement of battery dynamics was confirmed by the exchange current density in Fig. S10a (Supporting information). The j_0 increases from 0.079 mA/cm^2 (PP cell) to 0.508 mA/cm^2 (SZS-PP-SZS cell). The increase of j_0 and the decrease of $E_{a(RSEI)}$ show that the acid-base effect further accelerates the Li^+ through the SEI to participate in the interfacial electrochemical reaction. The result of cyclic voltammetry (CV) tests shows better redox reversibility of lithium iron phosphate batteries with the application of SZS-PP-SZS separators (Fig. S10b in Supporting information). The batteries after 3 cycles of activation were left and stored for different times (Fig. S11 in Supporting information). After 10 days, the R_{SEI} of the SZS-PP-SZS batteries only increases 0.936 Ω, while the R_{SEI} of the battery with PP separators increases 28.77 Ω. In comparison, the SEI stability of SZS-PP-SZS separator batteries is better.

Li||Li symmetric cells with PP or SZS-PP-SZS separators were charged and discharged at the constant current density to compare the long cycle performance. The symmetric cells with SZS-PP-SZS composite separators could operate stably for about 800 h when the polarization voltage was within 0.4 V (Fig. 4a). In contrast, the PP cells reaches polarization voltage of 0.4 V in less than 600 h and they are very unstable in later cycling. In addition, the polarization of the PP cells is very obvious at the beginning of the cycles due to their poor wettability. Increasing the current density, the polarization of the PP cells increases more significantly at high currents of 1 mA/cm^2 and 2 mA/cm^2, and their curves fluctuate significantly. While the SZS-PP-SZS cells still exhibit smaller polarization and more stable cycling (Figs. S12a and b in Supporting information). Cells assembled with SZS-PP-SZS modified separators exhibit superior cycling performance in long cycling, due to their better wettability, smaller concentration polarization, more efficient Li^+ migration, and stabler SEI. They also exhibit excellent rate performance (Fig. 4b).

The SEM characterization of the lithium anode morphology of the batteries was performed after completing a long cycling to

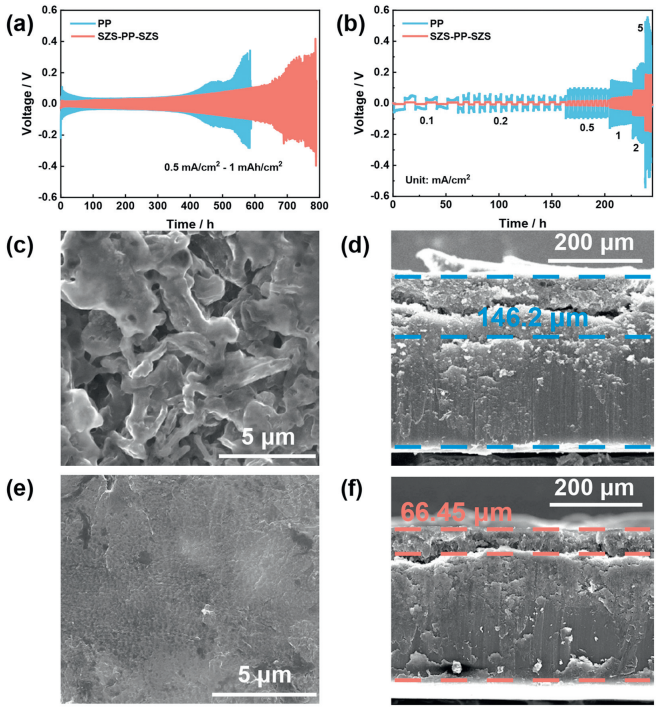

Fig. 4. (a) Cycling performance of the Li||Li cells with PP and SZS-PP-SZS separators under the current density of 0.5 mA/cm^2. (b) The rate performance of symmetric cells under the current density of 0.1, 0.2, 0.5, 1.0, 2.0, and 5.0 mA/cm^2 (all deposition capacity was 1.0 mAh/cm^2). Surface SEM images of lithium anodes in (c) PP and (e) SZS-PP-SZS cells after 100 cycles. SEM images about longitudinal section of lithium anode in (d) PP and (f) SZS-PP-SZS cells after 100 cycles.

compare the effect of the coating on the formation of lithium dendrites (Figs. 4c–f). The surfaces of the SZS-PP-SZS electrodes are relatively flat and the lithium deposition is more homogeneous after 100 cycles. While obvious lithium dendrites could be seen in the battery with PP separators. The thickness of the electrode surface layer is 146.2 μm in the cell with PP separators, which consisting of dead lithium, lithium dendrites, sparse lithium deposition layer and thick SEI (Fig. 4d). The thickness of the dense and smooth surface layer in the cell with SZS-PP-SZS modified separators is only 66.45 μm (Fig. 4f). As SZ immobilized PF_6^- anion through acid-base interaction, it increases Li^+ transference number and ion diffusion rate. This effect reduces the concentration polarization and allows rapid replenishment of lithium ions at the interfacial deposits. It makes the SEI membrane denser and more stable, and the lithium deposition is more uniform and transversal. This work inhibited the growth of lithium dendrites, as well as the formation and breakage of dead lithium, which further confirmed that modified separators had an enhanced effect on the cycling stability of the batteries.

The effect of SZS-PP-SZS separator modification on the suitability of the full cell was investigated by testing the performance of Li||LFP cell. We used the commercial $LiFePO_4$ electrodes with a surface loading of up to 14 mg/cm^2 as the cathode of the cell. The capacity retention of the SZS-PP-SZS full-cells is 90.7% after 120 cycles at 0.5 C, whereas the capacity of the PP cells decays completely after about 50 cycles (Fig. 5a). What is more, the test result at 1 C (Fig. 5b) shows that the SZS-PP-SZS batteries still have 82.0% capacity retention after 70 cycles. By contrast, the capacity of the PP batteries decreases sharply from the initial charging and discharging stage and decays to zero around the 40th cycle. We compared the charge/discharge curves of the two kinds of batteries under 1 C at the 5th and 20th cycles individually (Fig. 5c). The polarization voltage of the SZS-PP-SZS cells does not change much at the 5th and 20th cycles (both at about 0.46 V). However, the polarization voltage of the PP cells was 0.32 V higher than that of the SZS-PP-SZS in the 5th cycle, and the polarization voltage was even more obviously increased in the 20th cycle (up to 1.06 V). The Li||LFP full cell was disassembled to observe the changes of anode and cathode after 50 cycles at 0.5 C. The anode of the SZS-PP-SZS maintains an intact Li-metal luster (Fig. S13 in Supporting information). Meanwhile, the $LiFePO_4$ material on the cathode exhibits no change in structure and morphology before and after cycling (Fig. S15 in Supporting information).

The full cells assembled with two separators were conducted the rate performance tests at 0.1, 0.2, 0.5, 1 and 2 C (Fig. 5d). The specific capacity and charge/discharge efficiency of the two types of separators is akin under low rate and small current conditions. The specific capacity of the PP cells start to decrease after the rate is increased to 0.5 C, and the capacity decays cliff-like at 1 C. The SZS-PP-SZS cells could still provide a discharge specific capacity of about 96.6 mAh/g at 2 C. Furthermore, we compared the polarization condition of the charge/discharge curves at different rates (the uniform first cycle was taken as an example) (Figs. 5e and f). The polarization voltage of the SZS-PP-SZS cell at 0.5 C is about 0.369 V, which is lower than the PP cell (0.683 V). When the rate increase to 1 C, the polarization voltage of the SZS-PP-SZS cell is only 0.6978 V (PP cell is 1.533 V). The results show that applying

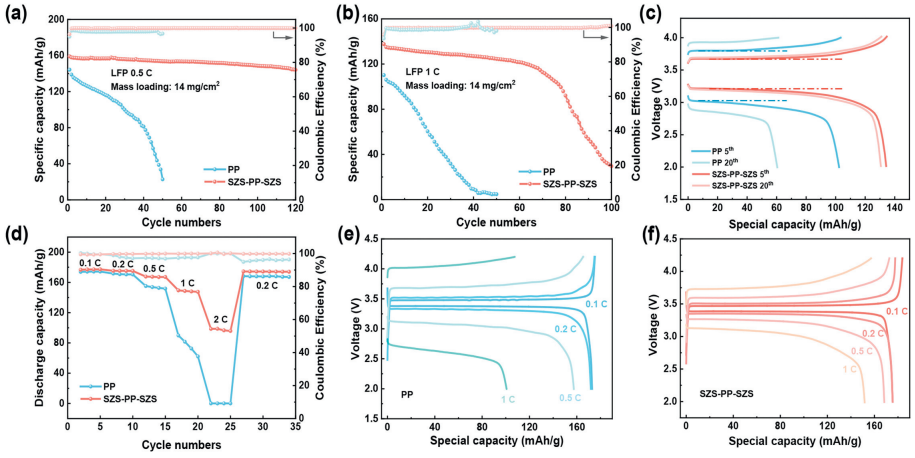

Fig. 5. Long cycle performance of Li||LFP cells at (a) 0.5 C and (b) 1 C. (c) Voltage-capacity profiles of Li||LFP cells at the 5th and 20th cycle. (d) Rate performance of Li||LFP cells. Voltage-capacity profiles of Li||LFP cells with (e) PP and (f) SZS-PP-SZS separators at the different rates.

the modified SZS-PP-SZS separators to lithium iron phosphate batteries can make the cycle more stably and provide better rate performance. They could resist high-current and high-rate charging and discharging. To summarize, the modification of lithium metal batteries by SZS-PP-SZS separators in terms of electrochemical performance has practical significance. That could also provide ideas for the development of LMB.

In this work, solid-acids were loaded onto molecular sieves to modify polypropylene separators. The study fully utilized the huge specific surface area of mesoporous molecular sieves to host and modulate solid-acids. The solid-acids further provided stronger acid active sites than the molecular sieve and played the principle of acid-base interaction to immobilize the PF_6^- anion. Modified separators facilitated the dissociation of lithium salts and the release of more lithium ions, thus promoting the uniform transport of ions. The SZS-PP-SZS separators effectively mitigated the deposition of lithium ions at the electrode tips and suppressed the formation of lithium dendrites. As a result, the batteries achieved over 800 h of stable low-polarization plating/stripping cycles. High mass loading lithium iron phosphate batteries with SZS-PP-SZS composite separators also demonstrated stable long-term cycling and enhanced rate performance. The effect of solid-acids provides prospect for the modification of lithium metal battery separators.

Declaration of competing interest

The authors declare that they have no known competing financial interests or personal relationships that could have appeared to influence the work reported in this paper.

CRediT authorship contribution statement

Ruofan Qi: Conceptualization, Data curation, Formal analysis, Investigation, Methodology, Software, Validation, Writing – original draft, Writing – review & editing. **Jing Zhang:** Writing – review & editing, Software. **Wang Sun:** Supervision, Writing – review & editing, Project administration, Resources. **Yu Bai:** Supervision, Writing – review & editing, Project administration, Methodology. **Zhenhua Wang:** Funding acquisition, Methodology, Resources, Supervision, Writing – original draft, Writing – review & editing, Project administration. **Kening Sun:** Funding acquisition, Project administration, Resources, Supervision.

Acknowledgment

This work was supported by the National Natural Science Foundation of China (No. 22179007).

Supplementary materials

Supplementary material associated with this article can be found, in the online version, at doi:10.1016/j.cclet.2024.110009.

References

[1] X. Cheng, C. Zhao, Y. Yao, et al., Chem 5 (2019) 74–96.
[2] J. Wang, B. Ge, H. Li, et al., Chem. Eng. J. 420 (2021) 129739.
[3] L. Zhang, C. Zhu, S. Yu, et al., J. Energy Chem. 66 (2022) 260–294.
[4] Z. Piao, R. Gao, Y. Liu, et al., Adv. Mater. 35 (2022) 2206009.
[5] Y. Liu, Z. Yu, J. Chen, et al., Chin. Chem. Lett. 33 (2022) 1817–1830.
[6] J. Du, X. Duan, W. Wang, et al., Nano Lett. 23 (2023) 3369–3376.
[7] X. Mao, L. Shi, H. Zhang, et al., J. Power Sources 342 (2017) 816–824.
[8] X. Cheng, S. Yang, Z. Liu, et al., Adv. Mater. 36 (2024) e2307370.
[9] M. Su, Y. Chen, S. Wang, et al., Chin. Chem. Lett. 34 (2023) 107553.
[10] F. Jiang, S. Yang, X. Cheng, et al., J. Energy Chem. 72 (2022) 158–165.
[11] S. Zhang, B. Cheng, Y. Fang, et al., Chin. Chem. Lett. 33 (2022) 3951–3954.
[12] Q. Zhao, R. Zhou, C. Wang, et al., Adv. Funct. Mater. 32 (2022) 2112711.
[13] T. Li, H. Liu, P. Shi, et al., Rare Metals 37 (2018) 449–458.
[14] X. Xu, S. Wang, H. Wang, et al., J. Energy Chem. 27 (2018) 513–527.
[15] M. Yang, Y. Ji, Y. Dong, et al., Chin. Chem. Lett. 34 (2023) 107087.
[16] J. Li, H. Jia, H. Li, et al., J. Energy Chem. 57 (2021) 61–68.
[17] M. Wang, J. Wang, J. Si, et al., Chem. Eng. J. 430 (2022) 132971.
[18] W. Ren, K. Zhu, W. Zhang, et al., Adv. Funct. Mater. 33 (2023) 2301586.
[19] T. Wei, J. Lu, P. Zhang, et al., Chin. Chem. Lett. 34 (2023) 107947.
[20] S.H. Choi, S.J. Lee, D.J. Yoo, et al., Adv. Energy Mater. 9 (2019) 1902278.
[21] W. Zhang, L. Wang, G. Ding, et al., Chin. Chem. Lett. 34 (2023) 107328.
[22] L. Xu, J. Yang, M. Huang, et al., Chem. Eng. J. 419 (2021) 129494.
[23] M. Zhang, R. Liu, Z. Wang, et al., Chin. Chem. Lett. 31 (2020) 1217–1220.
[24] M. Ge, X. Zhou, Y. Qin, et al., Chin. Chem. Lett. 33 (2022) 3894–3898.
[25] Q. Cheng, A. Li, N. Li, et al., Joule 3 (2019) 1510–1522.
[26] H. Xu, Y. Li, A. Zhou, et al., Nano Lett. 18 (2018) 7414–7418.
[27] X. Fan, X. Ji, F. Han, et al., Sci. Adv. 4 (2018) eaau9245.
[28] P. Wang, W. Qu, W. Song, et al., Adv. Funct. Mater. 29 (2019) 1900950.
[29] J. Liu, Y. Mo, S. Wang, et al., ACS Appl. Energy Mater. 2 (2019) 3886–3895.
[30] Z. Rong, Y. Sun, Q. Zhao, et al., Chem. Eng. J. 437 (2022) 135329.
[31] T. Lee, W.K. Kim, Y. Lee, et al., Macromol. Res. 22 (2014) 1190–1195.
[32] B.K. Park, H.S. Kim, S.A. Han, et al., ACS Appl. Mater. Interfaces 15 (2023) 6923–6932.
[33] H. Huo, X. Li, Y. Chen, et al., Energy Stor. Mater. 29 (2020) 361–366.
[34] L. Zhai, K. Yang, F. Jiang, et al., J. Energy Chem. 79 (2023) 357–364.
[35] X. Fu, C. Shang, M. Yang, et al., J. Power Sources 475 (2020) 228687.
[36] Y. Du, X. Gao, S. Li, et al., Chin. Chem. Lett. 31 (2020) 609–616.
[37] Y. Yang, S. Yao, Z. Liang, et al., ACS Energy Lett. 7 (2022) 885–896.
[38] X. Han, T. Wu, L. Gu, et al., Chin. Chem. Lett. 34 (2023) 107594.
[39] L. Chen, X. Lin, W. Dang, et al., Adv. Compos. Hybrid Mater. 6 (2022) 12.
[40] C. Zhao, P. Chen, R. Zhang, et al., Sci. Adv. 4 (2018) eaat3446.
[41] L. Zhao, Z. Wu, Z. Wang, et al., ACS Nano 16 (2022) 20891–20901.
[42] C. Zhang, L. Shen, J. Shen, et al., Adv. Mater. 31 (2019) 1808338.
[43] S.G. Woo, E.K. Hwang, H.K. Kang, et al., Energy Environ. Sci. 14 (2021) 1420–1428.
[44] Y. Lu, K. Korf, Y. Kambe, et al., Angew. Chem. Int. Ed. 53 (2014) 488–492.
[45] M.D. Tikekar, L.A. Archer, D.L. Koch, J. Electrochem. Soc. 161 (2014) A847.
[46] C. Zhao, X. Zhang, X. Cheng, et al., Proc. Natl. Acad. Sci. U. S. A. 114 (2017) 11069–11074.
[47] Y. Chen, P. Mickel, H. Pei, et al., ACS Appl. Mater. Interfaces 15 (2023) 18333–18342.
[48] Y. Hu, C. Wang, Y. Wu, et al., J. Mater. Chem. A 11 (2023) 12052–12061.
[49] P. Dong, X. Zhang, W. Hiscox, et al., Adv. Mater. 35 (2023) 2211841.
[50] Z. Hu, X. Zhang, S. Chen, J. Power Sources 477 (2020) 228754.
[51] Y. Nie, T. Yang, D. Luo, et al., Adv. Energy Mater. 13 (2023) 2204218.
[52] J. Zhang, Q. Fu, P. Li, et al., Particuology 89 (2024) 238–245.
[53] H. Su, H. Zhang, Z. Chen, et al., Chin. Chem. Lett. 34 (2023) 108640.
[54] J. Liang, S. Sun, N. Yao, et al., Sci. China Chem. 66 (2023) 3620–3627.
[55] J.X. Chen, J.H. Zhang, X.Z. Fan, et al., Energy Environ. Sci. 17 (2024) 4036–4043.
[56] A. Eftekhari, Micropor. Mesopor. Mat. 243 (2017) 355–369.
[57] H. Xie, Z. Hao, S. Xie, et al., Nano Res. 15 (2022) 5143–5152.
[58] J. Xiao, Q. Li, Y. Bi, et al., Nat Energy 5 (2020) 561–568.